Arabian Journal of Chemistry (2020) **13**, 6395–6402

King Saud University

Arabian Journal of Chemistry

www.ksu.edu.sa
www.sciencedirect.com

ORIGINAL ARTICLE

NMR investigation of substituent effects on strength of π-π stacking and hydrogen bonding interactions to supports the formation of [2 + 2] photodimerization in (para-X-ba):::(bpe)||(bpe):::(para-X-ba) complexes

Solmaz Abdolahi Jonghani, Zeinab Biglari *, Alireza Gholipour *

Department of Chemistry, Faculty of Science, LorestanUniversity, Khoramabad, Iran

Received 21 March 2020; accepted 31 May 2020
Available online 10 June 2020

KEYWORDS

Photodimerization;
Computational chemistry;
Hammett constants;
π-π Stacking;
Hydrogen bonding

Abstract We have investigated the ability of para-X-phenylboronic acid (para-X-ba) to enable reactivity of trans-1,2-bis(4-pyridyl)ethylene (bpe) to direct intermolecular [2 + 2] photodimerization via computational chemistry. Para-X-ba would support the formation of discrete four component hydrogen bonded molecular assemblies wherein π-π stacking of a pyridyl-functionalized alkene would conform to undergo [2 + 2] photodimerization.

We have demonstrated by computational ^{1}H NMR data the effect of electron-withdrawing and donating substituents in (para-X-ba):::(bpe)||(bpe):::(para-X-ba) complexes to assemble bpe into π-π stacking via –(B)O − H···N– hydrogen bonds to react to afford (para-X-ba):::tpcb:::(para-X-ba) complexes (X = NO2, CN, F, Cl, Br, C(O)CH_3, OCH_3, OH, NH_2 and H where || and ••• denote π-π stacking and hydrogen bonds).

Also, these interactions have been investigated at M05-2X/6-311 + + G** level of theory in detail in terms of the energetic, geometrical parameters and electron density properties to characterize and to examine the strengthening of the interactions. There are good relationships between the NMR, AIM, energy data and Hammett constants.

1. Introduction

Boronic acids have been widely used as reagents for the targeted synthesis of compounds having applications in the areas of pharmaceuticals, agrochemicals etc. It should be noted that there are potential drawbacks to using boronic acids as supramolecular building blocks, especially in the presence of

* Corresponding authors.
E-mail addresses: biglari.z@lu.ac.ir, biglariz@gmail.com (Z. Biglari), Gholipour.a@lu.ac.ir, Alir.gholipour@gmail.com (A. Gholipour).

Peer review under responsibility of King Saud University.

ELSEVIER Production and hosting by Elsevier

https://doi.org/10.1016/j.arabjc.2020.05.040
1878-5352

heterocyclic compounds (Zheng et al., 2010, 2012; Das et al., 2017; Cuenca et al., 2016; Hall, 2006; Li et al., 2017; Diemoz and Franz, 2019). Boronic acids can be regarded as "green" compounds due to their low toxicity and their ultimate degradation into the environmentally friendly boric acid (Hall, 2005). The reversible hydrogen bonding interactions that boronic acids can take part in has seen a significant increase in the applications of boronic acid based systems in self-assembly sensing, and separation science (James, 2016; Nishiyabu et al., 2011; Kubo et al., 2015; Fujita et al., 2008; Corbett et al., 2006). While there has been considerable work on the construction of supramolecular frameworks and architectures based on organoboronic acids; (Saleem et al., 2019; Chen et al., 2020) there has been significantly less work on the ability of boronic acids to form hydrogen-bonded complexes.

The evidence for the formation of hydrogen bonds and π-π stacking in boronic acids is substantial and its relevance at the solid state has been essentially limited to the self-associated architectures and data regarding the thermodynamics of the interactions with complementary recognition motifs in solution are essentially unknown (Shang et al., 2015; Zhao et al., 2016; Iribarren et al., 2019; Campos-Gaxiola et al., 2010; Rettig and Trotter, 1977; Cyrański et al., 2008). These interactions are among the most prevalent non-covalent interactions present in both natural systems and synthetic (Meyer et al., 2003; Burley and Petsko, 1985). These interactions play an important role in determining the conformation of organic molecules, (Hughes and Waters, 2006) the structure and stability of proteins, and directing the stereoselectivity of organic transformations (Pecsi et al., 2010).

To the best of our knowledge, we have investigated the ability of para-X-ba where: X = NO_2, CN, F, Cl, Br, $C(O)CH_3$, OCH_3, OH, NH_2 and H to enable reactivity of trans-1,2-bis (4-pyridyl)ethylene (bpe) to direct intermolecular [2 + 2] photodimerization via computational chemistry (Scheme 1). Para-X-ba would support the formation of discrete four-component hydrogen-bonded molecular assemblies wherein π-π stacking of a pyridyl-functionalized alkene would conform to undergo [2 + 2] photodimerization.

Our efforts to utilize the complexes based on para-X-ba to enable photoreactivity of bpe are inspired by work of MacGillivray et Al. (Alvarado et al., 2018) who experimentally demonstrated a propensity of related para-X-ba and bpe to assemble by a combination of π-π stacking contacts and hydrogen bond interactions. The work of MacGillivray et al. (Alvarado et al., 2018) prompted us to explore potential to employ para-X-ba to direct an intermolecular [2 + 2] photodimerization of bpe by computational chemistry.

2. Computational chemistry

To shed further light on the electronic and geometries properties ruling the formation and the stability of the (para-X-ba):::(bpe)||(bpe):::(para-X-ba) and (para-X-ba):::tpcb:::(para-X-ba) complexes (X = NO_2, CN, F, Cl, Br, $C(O)CH_3$, OCH_3, OH, NH_2 and H where || and ••• denote π-π stacking and hydrogen bonds), DFT geometry optimization and frequency calculations were carried out at the M05-2X/6–311 + + G** level (Zhao and Truhlar, 2008) using the GAMESS program (Schmidt et al., 1993). The geometries have been optimized using the the gradient CP-corrected methods (Boys and Bernardi, 1970). Calculations were followed by harmonic vibrational frequencies calculations at the same level of theory and it confirms that the optimized structures have energetic minima on their potential energy surfaces.

In following, the ^{1}HNMR calculations of the chemical shielding were performed for structure of the complexes. The chemical shielding of protons were computed at M05-2X/6–311 + + G** levels using SPINSPIN keyword. The shielding values were used to calculate the chemical shifts of hydrogen with respect to TMS ($\delta_H = \sigma_{TMS} - \sigma_H$). Also, we employed the nucleus independent chemical shift (NICS) index that is one of the most widely employed indicators of aromaticity, which was proposed by Schleyer and co-workers (Ebrahimi et al., 2009a, 2009b; Ghafari and Gholipour, 2015, 2019; Schleyer and Jiao, 1996; Schleyer et al., 1996; Biegler Konig et al., 2001; Hammett, 1935; Zhu et al., 2003; Zhikol et al., 2005; Quinonero et al., 2008). It is defined as the negative value of the absolute shielding computed at a ring center.

The wave functions at the M05-2X/6–311 + + G** level were used to examine the electron density within the atoms in molecules (AIM) methodology by using the AIM2000 program (Biegler Konig et al., 2001).

3. Results and discussion:

We computationally demonstrated the ability of para-X-phenylboronic acid (para-X-ba) to assemble trans-1,2-bis (4-pyridyl)ethylene (bpe) into π-π stacks via –(B)O − H···N– hydrogen bonds in (para-X-ba):::(bpe)||(bpe):::(para-X-ba) complexes to react to afford rctt-tetrakis(4-pyridyl)cyclobutane (tpcb), (para-X-ba):::tpcb:::(para-X-ba) complexes (Scheme 1). We demonstrated para-X-ba in (para-X-ba):::(bpe)||(bpe):::(para-X-ba) complexes to act as a bifunctional hydrogen-bond-donor template by assembling bpe by way of –(B)O − H···N– hydrogen bonds in a discrete four-component supramolecular assembly to undergo an intermolecular [2 + 2] photodimerization. This photocycloaddition reaction generates (para-X-ba):::tpcb:::(para-X-ba) complexes. The components of (para-X-ba):::(bpe)||(bpe):::(para-X-ba) complexes as discrete four-component molecular assemblies sustained by four –(B)O − H···N– hydrogen bonds and π-π stacks of bpe have enabled the C = C bonds to be stacked in a suitable geometry for a [2 + 2] photodimerization (Scheme 1).

The results summarized in Table 1 allow us to analyze the electronic effects of substituents in terms of the Hammett constant (Hammett, 1935). Hammett constants of substituents demonstrated that electron-donating or electron-withdrawing substituent (X) influence π-π stacking the hydrogen bond interactions in (para-X-ba):::(bpe)||(bpe):::(para-X-ba) and (para-X-ba):::tpcb:::(para-X-ba) complexes. The electron-donating or electron-withdrawing capabilities of substituents which are including were describes using Hammett constant and the trend in electron withdrawing strength was found to be: NH_2 < OH < OCH_3 < H < F < Cl < Br < $C(O)CH_3$ < CN < NO_2.

The corresponding binding energies of complexes were evaluated using Eq. (1) and are also tabulated in Table 1.

$$E = Ecomplexes - \sum_{i=1}^{4} E_{monomer(i)} \quad (1)$$

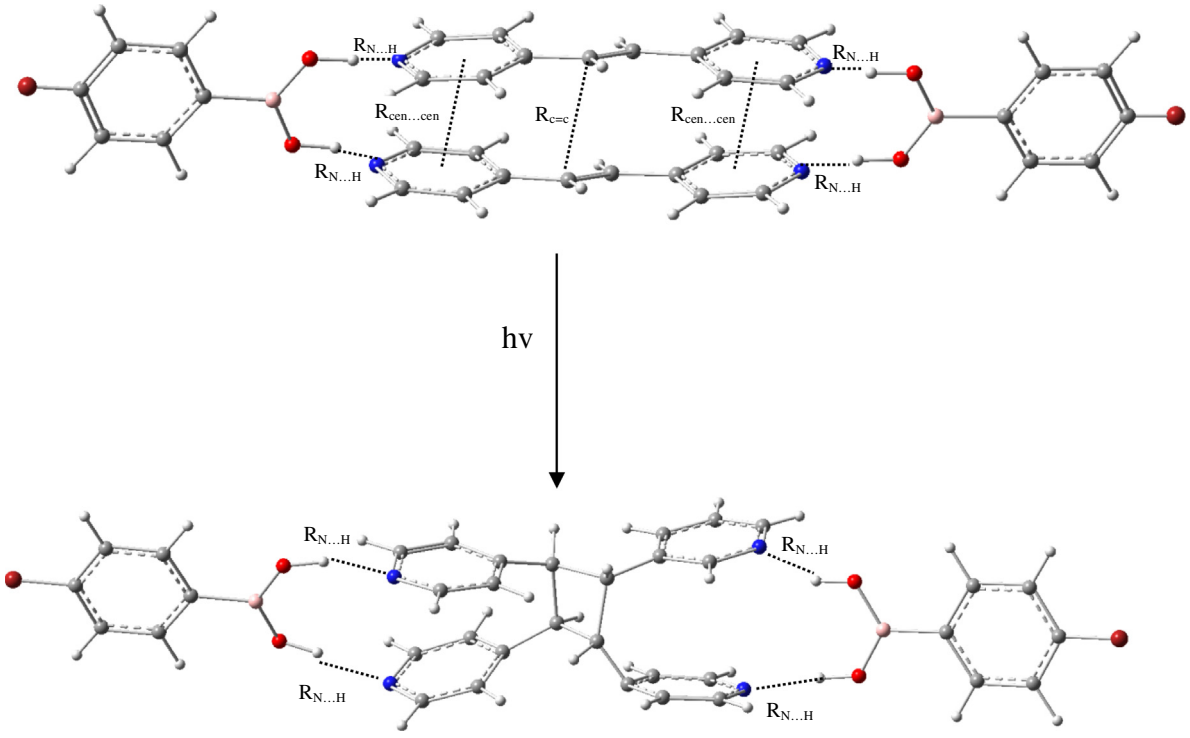

Scheme 1 Molecular models used in the present study. (Red spherical = NO_2, CN, $C(O)OCH_3$, F, Cl, Br, H, OCH_3 OH and NH_2 substituents).

Table 1 The The ΔE (kcal mol^{-1}). The most important geometrical parameters (in Å) for (para-X-ba):::(bpe)||(bpe):::(para-X-ba) and (para-X-ba):::tpcb:::(para-X-ba) complexes calculated at M05-2X/6–311 + + G** level of theory.

	(para-X-ba):::(bpe)||(bpe):::(para-X-ba)				(para-X-ba):::tpcb:::(para-X-ba)		
X	ΔE	$R_{N...H}$	$R_{cen...cen}$	$R_{c=c}$	ΔE	$R_{N\cdots H}$	σ_{total}
NO_2	-38.84	1.928	3.670	3.896	-26.02	2.093	1.48
CN	-38.34	1.933	3.664	3.895	-25.64	2.102	1.26
$C(O)CH_3$	-37.14	1.949	3.621	3.893	-24.92	2.114	0.82
Br	-37.02	1.950	3.620	3.892	-24.70	2.121	0.69
Cl	-36.59	1.952	3.595	3.892	-24.46	2.120	0.61
F	-36.28	1.956	3.581	3.892	-24.27	2.126	0.49
H	-35.51	1.963	3.573	3.889	-23.63	2.143	0.00
OH	-35.25	1.971	3.565	3.887	-23.69	2.154	-0.25
OCH_3	-34.92	1.975	3.550	3.884	-23.41	2.158	-0.15
NH_2	-34.10	1.983	3.510	3.882	-22.93	2.169	-0.82

The increase in ΔE arises in (para-X-ba):::(bpe)||(bpe):::(para-X-ba) and (para-X-ba):::tpcb:::(para-X-ba) complexes with the electron withdrawing substituents (see Table 1). Whereas ΔE is in the range from −38.84 to −34.09 kcal/mol for (para-X-ba):::(bpe)||(bpe):::(para-X-ba) and from −26.01 to −22.92 kcal/mol for (para-X-ba):::tpcb:::(para-X-ba) complexes. The binding energy from NH_2 to NO_2 is in the following order: NH_2 < OCH_3 < OH < H < F < Cl < Br < $C(O)CH_3$ < CN < NO_2. The binding energy is more as manifested in the largest ΔE values in $–NO_2$ substituent compared to other substituents.

The lowest values ΔE are found for–NH_2 substituent that is equal to −34.10 and –22.92 $kcalmol^{-1}$ to (para-X-ba):::(bpe)||(bpe):::(para-X-ba) and (para-X-ba):::tpcb:::(para-X-ba) complexes, respectively.

The constants σ_{para} or σ_{meta} are not effective parameters to describe intermolecular interactions in these complexes. Therefore, both para and meta positions, that are, σ_{para} and σ_{meta}, certainly have an effect on the binding energies so new parameter σ_{total} (σ_{total} = (σ_{para} + σ_{meta})) was applied to describe these interactions (see Table 1) (Ghafari and Gholipour, 2015, 2019; Zhu et al., 2003; Ebrahimi et al., 2009). Increasing binding energies with electron withdrawing character of substituents show a meaningful correlation between the Hammett constant of substituents and the interaction energies of (para-X-ba):::(bpe)||(bpe):::(para-X-ba) and (para-X-ba):::tpcb:::(para-X-ba) complexes. We demonstrated the correlation between the Hammett's parameter and the value of ΔE (Fig. 1).

4. Geometrical parameters

The geometrical data of all the optimized complexes included in this study were gathered in Table 1 at the M05-2X/6–311 + + G** level of theory which is contained $R_{N\cdots H}$, $R_{cen\cdots cen}$ and $R_{C=C}$ geometrical parameters (see Scheme 1). Selected geometrical parameters for the related complexes are represented in Scheme 1. The $R_{N\cdots H}$, $R_{cen\cdots cen}$ and $R_{C=C}$ geometrical parameters are selected to derive the general trend of the relative strength of these interaction. $R_{N\ldots H}$ is the -(B)O − H··· N- intermolecular hydrogen bond distance between para-X-ba and bpe molecule. $R_{cen\cdots cen}$ is the distance between the center of pyridine rings in two bpe molecules;. $R_{C=C}$ is the distance between the C = C bonds stacked in two bpe molecules.

As it can be seen from Scheme 1, para-X-ba are connected to two bpe molecules through –(B)O − H···N– hydrogen bonds. Substitutions of the studied complexes result in essentially change in the $R_{N\ldots H}$ hydrogen bond lengths (see Table 1). The four $R_{N\ldots H}$ hydrogen bond distances of each substitute have almost the same length. The $R_{N\ldots H}$ distances found range from 1.928 to 1.983 Å (mean value) for complexes (para-X-ba):::(bpe)||(bpe):::(para-X-ba) and from 2.093 to 2.169 Å (mean value) for (para-X-ba):::tpcb:::(para-X-ba) complexes. As can be seen in Table 1, the $R_{N\cdots H}$ for these complexes increases with increasing electron-donating character of substituents.

An electron-withdrawing substituent tends to decrease the $R_{N\ldots H}$ in complexes in comparison with other substituents and this quantity increases through the incorporation of an electron- donating substituent. As depicted in Table 1, this observation signifies that $R_{N\ldots H}$ for (X = NH_2) complex is greater than any other complexes and this quantity in (X = NO_2) complex is shorter than those of the corresponding complexes. The $R_{N\ldots H}$ falls in the order NH_2 > OCH_3 > OH > H > F > Cl > Br > $C(O)CH_3$ > CN > NO_2. We demonstrated the correlation between the $R_{N\ldots H}$ and the value of ΔE (Fig. 2).

The information on the geometry (i.e. $R_{N\ldots H}$, $R_{cen\cdots cen}$ and $R_{C=C}$) were important in the complexes, thus, $R_{cen\cdots cen}$ and $R_{C=C}$ of bpe molecules are suitable geometry parameters for strength of π-π stacking interaction. The π-π stacking of the bpe molecule would place the C = C bonds in positions to undergo intermolecular [2 + 2] photodimerizations in (para-X-ba):::(bpe)||(bpe):::(para-X-ba) complexes.

The $R_{cen\cdots cen}$ distances found range from 3.670 to 3.609 Å (mean value) (para-X-ba):::(bpe)||(bpe):::(para-X-ba) complexes. Inspection of the data in Table 1 shows that the distant between center of pyridine rings in (para-X-ba):::(bpe)||(bpe):::(para-X-ba) complexes ($R_{cen\cdots cen}$) is affected by the substituents. Noteworthy, $R_{cen\cdots cen}$ of the π-π stacking interaction can be reduced by the electron donating substituents, the lowest $R_{cen\text{-}cen}$ is observed for (para-X-ba):::(bpe)||(bpe):::(para-X-ba) complexes (X = NH_2) (see Table 1), also in agreement with the energy analysis, the trend in the $R_{cen\cdots cen}$ is: NH_2 < $C(O)CH_3$ < H < Br < F < Cl < OCH_3 < OH < CN < NO_2. Table 1 shows that (para-X-ba):::(bpe)||(bpe):::(para-X-ba) complexes have shorter $R_{cen\text{-}cen}$ which increases with increasing electron- withdrawing character of the substituents, and a reverse behavior is shown for electron- donating substituents. It is largest in (para-NO_2-ba):::(bpe)||(bpe):::(para-NO_2-ba) complex and smallest in (para-NH_2-ba):::(bpe)||(bpe):::(para-NH_2-ba) complex.

The $R_{C=C}$ distances found range from 3.896 to 3.882 Å (mean value) (para-X-ba):::(bpe)||(bpe):::(para-X-ba) complexes. Inspection of the data in Table 1 shows that the distant between center of pyridine rings in (para-X-ba):::(bpe)||(bpe):::(para-X-ba) complexes ($R_{C=C}$) is affected by the substituents. The lowest $R_{cen\text{-}cen}$ is observed for (para-X-ba):::(bpe)||(bpe):::(para-X-ba) complexes (X = NH_2) (see Table 1), also in agreement with the energy analysis, the trend in the $R_{C=C}$ is: NH_2 < $C(O)CH_3$ < H < Br < F < Cl < OCH_3 < OH < CN < NO_2. Table 1 shows that (para-X-ba):::(bpe)||(bpe):::(para-X-ba) complexes have shorter $R_{C=C}$ which increases with increasing electron- withdrawing character of the substituents, and a reverse behavior is shown for electron- donating substituents. It is largest in (para-NO_2-ba):::(bpe)||(bpe):::(para-NO_2-ba) complex and smallest in (para-NH_2-ba):::(bpe)||(bpe):::(para-NH_2-ba) complex.

5. NMR spectroscopy

The NMR analysis will be carried out to understand chemical shielding of $\delta_{N\text{-}H}$, δ_{Ha}, δ_{Hb} δ_{Hc}, $\delta_{Ha'}$, $\delta_{Hb'}$ and δ_{Hf} proton that gathered in Table 2 for (para-X-ba):::(bpe)||(bpe):::(para-X-ba)

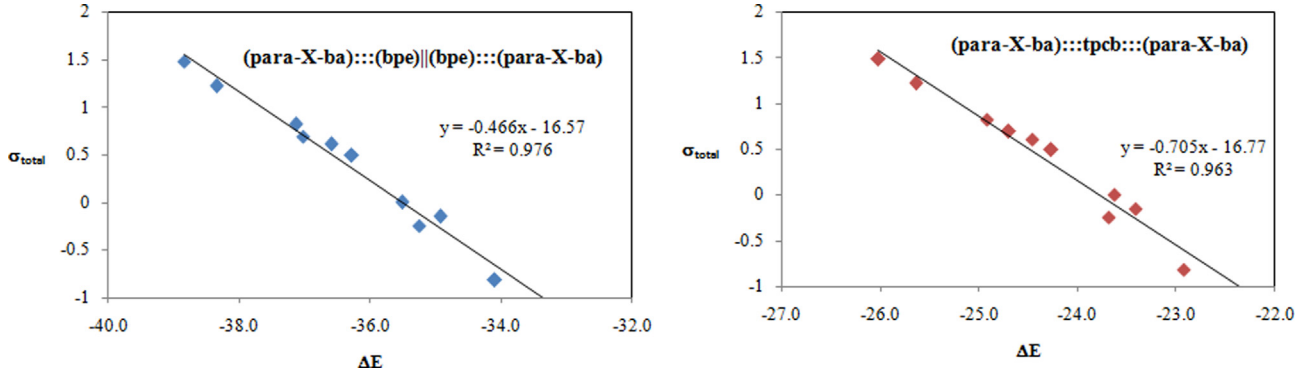

Fig. 1 Correlation between ΔE and Hammett constant σ_{total} for (para-X-ba):::(bpe)||(bpe):::(para-X-ba) (left) and (para-X-ba):::tpcb:::(para-X-ba) (right) complexes.

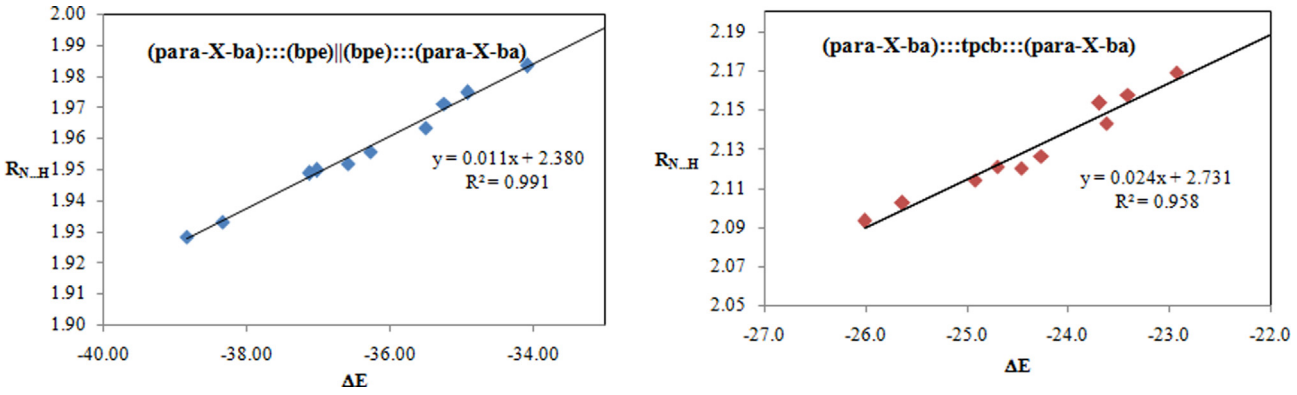

Fig. 2 Correlation between ΔE and $R_{N\ldots H}$ for (para-X-ba):::(bpe)||(bpe):::(para-X-ba) (left) and (para-X-ba):::tpcb:::(para-X-ba) (right) complexes.

Table 2 Shielded N-H, H^a, H^b, H^c, $H^{a'}$, $H^{b'}$, H^f proton values and aromaticity at for para-X-ba in (para-X-ba):::(bpe)||(bpe):::(para-X-ba) and (para-X-ba):::tpcb:::(para-X-ba) complexes calculated at M05-2X/6–311 + + G** level of theory.

X	(para-X-ba):::(bpe)||(bpe):::(para-X-ba)					(para-X-ba):::tpcb:::(para-X-ba)				
	$\delta_{N\text{-}H}$	δ_{Ha}	δ_{Hb}	δ_{Hc}	NICS(1)	$\delta_{N\text{-}H}$	$\delta_{Ha'}$	$\delta_{Hb'}$	δ_{Hf}	NICS(1)
NO_2	8.77	7.90	7.46	7.68	−11.01	7.07	8.32	6.69	4.56	−10.82
CN	8.63	7.99	7.60	7.78	−10.75	6.76	8.35	6.66	4.53	−10.63
$C(O)CH_3$	8.32	8.02	7.56	7.86	−10.21	6.43	8.38	6.62	4.56	−10.36
Br	8.26	8.05	7.54	7.73	−10.28	6.19	8.39	6.62	4.52	−10.14
Cl	8.26	8.08	7.56	7.76	−10.37	6.26	8.40	6.63	4.51	−10.29
F	8.12	8.91	7.46	7.66	−10.08	6.11	8.42	6.63	4.53	−10.02
H	8.13	9.46	7.83	7.75	−10.11	5.88	9.37	7.94	4.57	−9.84
OH	7.81	9.51	7.80	7.75	−9.61	5.63	8.52	8.00	4.52	−10.01
OCH_3	7.94	9.51	7.78	7.75	−10.00	5.51	9.32	6.72	4.52	−9.93
NH_2	7.68	8.97	7.40	7.63	−9.38	5.29	8.58	6.74	4.55	−9.63

and (para-X-ba):::tpcb:::(para-X-ba) complexes with electron withdrawing and donating substituents at M05-2X/6–311 + + G** level of theory. The strength of the hydrogen bonding interactions was explained when setting the electron withdrawing and donating substituents by NMR data. For direct comparison of the ^1H shielding values, we calculated the same for H atoms of tetramethyl silane (TMS) at the same level of theory ($\delta_H = \sigma_{TMS} - \sigma_H$). For TMS protons, NMR shielding appears at 31.62 ppm.

The $\delta_{N\text{-}H}$ values are presented in Table 2 that have found range from 7.68 to 8.77 ppm (mean value) for complexes (para-X-ba):::(bpe)||(bpe):::(para-X-ba) and 5.29–7.07 ppm (mean value) for (para-X-ba):::tpcb:::(para-X-ba) complexes, respectively. The variation of $\delta_{N\text{-}H}$ can be characterized as the effect of the substituents by influencing –(B)O − H···N– bond that results in stabilization of hydrogen bonding (Table 2).

In order to study the influence of the substituents on the H shielding, the value of H shielding in substituted complexes has been calculated. This hydrogen bonding in (para-X-ba):::(bpe)||(bpe):::(para-X-ba) and (para-X-ba):::tpcb:::(para-X-ba) complexes manifests itself by a shielded N-H proton signal. The influence of the electron withdrawing and the electron-donating substituents on the $\delta_{N\text{-}H}$ is observed and presented in Table 2. The (para-X-ba):::(bpe)||(bpe):::(para-X-ba) and (para-X-ba):::tpcb:::(para-X-ba) complexes with electron withdrawing substituents have a larger $\delta_{N\text{-}H}$. In particular, the $\delta_{N\text{-}H}$ decreases for these complexes which bear an electron-donation substituent (Table 2). The largest magnitude of $\delta_{N\text{-}H}$ correspond to $–NO_2$ electron donating substituent that is equal to 8.77 and 7.07 ppm in (para-X-ba):::(bpe)||(bpe):::(para-X-ba) and (para-X-ba):::tpcb:::(para-X-ba) complexes, respectively. We see from Table 2 that in fact $\delta_{N\text{-}H}$ is lowest for NH_2 substituent with the values of 7.68 and 5.29 ppm for (para-X-ba):::(bpe)||(bpe):::(para-X-ba) and (para-X-ba):::tpcb:::(para-X-ba) complexes, respectively. The reduction of –(B)O − H··· N– hydrogen bonds distances is also accompanied by increasing H shielding in complextion. The minimum value of H shielding is accompanied by the highest $R_{N\ldots H}$ hydrogen bond lengths.

The δ_{Ha}, δ_{Hb} δ_{Hc}, $\delta_{Ha'}$, $\delta_{Hb'}$ and δ_{Hf} of (para-X-ba):::(bpe)||(bpe):::(para-X-ba) and (para-X-ba):::tpcb:::(para-X-ba) complexes were calculated by ab initio method at the M05-2X/6–311 + + G** level of theory (see Scheme 2), which shows features in reasonable agreement with experimental data (Alvarado et al., 2018). The δ_{Ha};δ_{Hb} δ_{Hc}, $\delta_{Ha'}$, $\delta_{Hb'}$ and δ_{Hf} are also changed due to influence of the electron withdrawing and donating substituents that summarized in Table 2.

The nucleus independent chemical shift (NICS) index is one of the most widely employed indicators of aromaticity, which was proposed by Schleyer and co-workers (Chen et al.; Schleyer and Jiao, 1996; Schleyer et al., 1996). It is defined

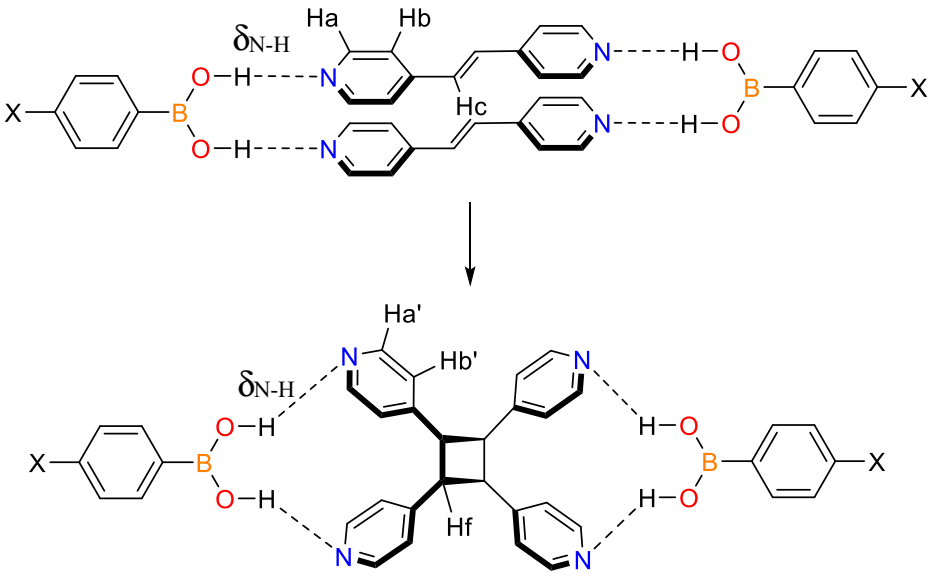

Scheme 2 The $\delta_{N\text{-}H}$, δ_{Ha}, δ_{Hb} δ_{Hc}, $\delta_{Ha'}$, $\delta_{Hb'}$ and δ_{Hf} of (para-X-ba):::(bpe)||(bpe):::(para-X-ba) and (para-X-ba):::tpcb:::(para-X-ba) complexes.

as the negative value of the absolute shielding computed at a ring center.

We have also studied the aromatic character of para-X-ba by means of NICS calculations. the aromaticity of the para-X-ba acid in (para-X-ba):::(bpe)||(bpe):::(para-X-ba) and (para-X-ba):::tpcb:::(para-X-ba) complexes changes when para-X-ba participate in hydrogen bonding interactions. There are observed changes in aromaticity of these complexes by predictions of NICS due to electron withdrawing and donating substituents. NICS(1) (1 Å above the plane of the ring) essentially reflects π effects. The electron withdrawing and donating effect of the substituent manifests itself by increasing and decreasing the aromaticity of para-X-ba ring in the (para-X-ba):::(bpe)||(bpe):::(para-X-ba) and (para-X-ba):::tpcb:::(para-X-ba) complexes, it is apparent that X = NO_2 in these complexes has the largest NICS(1). If we compare the NICS(1) of (para-X-ba):::(bpe)||(bpe):::(para-X-ba) and (para-X-ba):::tpcb:::(para-X-ba) complexes with different substituents, we can see that the $–NH_2$ substituent have lowest one.

The NICS values are presented in Table 2 that have found range from −9.38 to −11.01 ppm for (para-X-ba):::(bpe)||(bpe):::(para-X-ba) complexes and from −9.63 to −10.82 ppm for (para-X-ba):::tpcb:::(para-X-ba) complexes, respectively. We demonstrated the correlation between the NICS and the value of $\delta_{N\text{-}H}$. (Fig. 3).

6. AIM analysis

To rationalize the observed trends, the electron density at bond critical points (ρ_{BCP}) and at cage critical points (ρ_{CCP}) of computed (para-X-ba):::(bpe)||(bpe):::(para-X-ba) and (para-X-ba):::tpcb:::(para-X-ba) complexes were performed using the AIM analysis at M05-2X/6–311++G** level together with QTAIM that reported in Table 3. The effect of substituents on the hydrogen bonds was completely surveyed by the electron density at bond critical points ρ_{BCP} (Table 3). The ρ_{BCP} values are presented in Table 3 that have found range from 5.128 to 5.947 a.u (mean value) for complexes (para-X-ba):::(bpe)||(bpe):::(para-X-ba) and from 2.799 to 3.445 a.u (mean value) for (para-X-ba):::tpcb:::(para-X-ba) complexes, respectively.

Comparison of ρ_{BCP} indicates that the largest magnitude of ρ_{BCP} occurred in the presence of $–NO_2$ substituent and the lowest value of ρ_{BCP} is related to $–NH_2$ complex, as given in Table 3. The ρ_{BCP} varies in the order: NH_2 < OCH_3 < OH < H < F < Cl < Br < C(O)CH3 < CN < NO_2. This trend can be expected because the strength decreases from electron withdrawing to electron donating substituents.

The ρ_{BCP} was well correlated with the ΔE, in summary, as the electron density ρ_{BCP} increases, there is seen a significant enhancement in the binding energies ΔE. The ρ_{BCP} and interaction energy of these molecules also reveal the same trend (see Tables 1 and 3).

The ρ_{BCP} is at a maximum in NO_2 substituent that presents the shortest -(B)O − H···N- hydrogen bonds distances, confirming that the ρ_{BCP} at the bond critical points is a good indicator of the strength of the interaction. In other words, the -(B)O − H···N- hydrogen bonds weakening can be reflected from a decrease in ρ_{BCP}.

The electron density at cage critical points (ρ_{CCP}) is in good correlation with strength of π-π stacking interaction which was previously reported (Ebrahimi et al., 2009; Zhikol et al., 2005; Quinonero et al., 2008). To explain the strength of π-π stacking interaction, the ρ_{CCP} was applied to give reliable results about strength and stabilization of this interaction. The increase in ρ_{CCP} is a direct consequence of the presence of electron withdrawing substituents, which predicts that electron withdrawing substituents have reinforced effects on (para-X-ba):::(bpe)||(bpe):::(para-X-ba) complexes (Table 3). The lowest value of ρ_{CCP} is attributed to the NH_2 and NO_2 substituent exhibit largest values of ρ_{CCP} than the corresponding ρ_{CCP} for other substituents. The results also indicate that the NO_2 substituent apparently enhances the π-π stacking interaction.

The results obtained for the Laplacian ($\nabla^2\rho$), potential energy density, V(r) and the energy density (H) at the critical

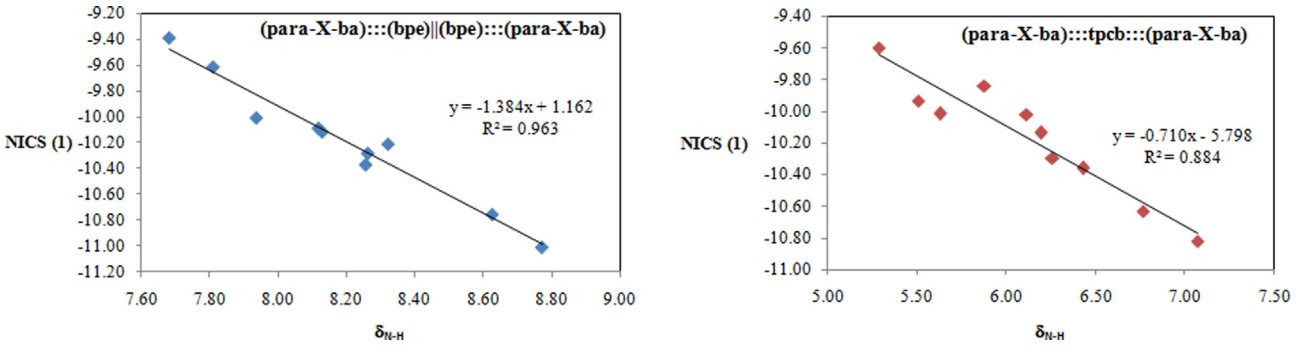

Fig. 3 Correlation between $\delta_{N\text{-}H}$ and NICS(1) for (para-X-ba):::(bpe)||(bpe):::(para-X-ba) (left) and (para-X-ba):::tpcb:::(para-X-ba) (right) complexes.

Table 3 Electron densities-ρ (in e/a_0^3), laplacians of electron densities-$\nabla^2\rho$ (in e/a_0^5), energy density (H) and potential energy density V(r) at -N···H- BCP for (para-X-ba):::(bpe)||(bpe):::(para-X-ba) and (para-X-ba):::tpcb:::(para-X-ba) complexes and Electron densities-ρ (in e/a_0^3), laplacians of electron densities-$\nabla^2\rho$ (in e/a_0^5), energy density (H) and potential energy density V(r) at CCP for (para-X-ba):::(bpe)||(bpe):::(para-X-ba) complexes calculated at M05-2X/6–311 + + G** level of theory. The ρ and $\nabla^2\rho$ data multiplied by 10^2.

	(para-X-ba):::(bpe)‖(bpe):::(para-X-ba)							(para-X-ba):::tpcb:::(para-X-ba)			
X	ρ_{BCP}	$\nabla^2\rho_{BCP}$	*H*	*V(r)*	ρ_{CCP}	$\nabla^2\rho_{BCP}$	*H*	*V(r)*	ρ_{BCP}	$\nabla^2\rho_{BCP}$	*H*	*V(r)*
NO_2	5.947	2.875	-0.047	0.671	0.772	0.561	-0.016	0.127	3.445	1.310	-0.016	0.321
CN	5.881	2.838	-0.049	0.660	0.771	0.560	-0.017	0.126	3.361	1.332	-0.017	0.318
$C(O)CH_3$	5.878	2.766	-0.056	0.635	0.757	0.559	-0.018	0.125	3.233	1.340	-0.019	0.315
Br	5.763	2.730	-0.057	0.624	0.769	0.558	-0.019	0.125	3.176	1.352	-0.020	0.312
Cl	5.621	2.725	-0.058	0.622	0.770	0.557	-0.019	0.122	3.163	1.365	-0.021	0.310
F	5.599	2.696	-0.059	0.614	0.765	0.555	-0.020	0.121	3.116	1.401	-0.022	0.305
H	5.506	2.618	-0.063	0.590	0.759	0.553	-0.020	0.119	2.991	1.440	-0.023	0.301
OH	5.378	2.577	-0.063	0.580	0.766	0.552	-0.021	0.118	2.935	1.551	-0.024	0.295
OCH_3	5.335	2.537	-0.064	0.571	0.765	0.551	-0.021	0.117	2.880	1.556	-0.025	0.297
NH_2	5.218	2.479	-0.065	0.556	0.754	0.550	-0.020	0.115	2.799	1.654	-0.028	0.295

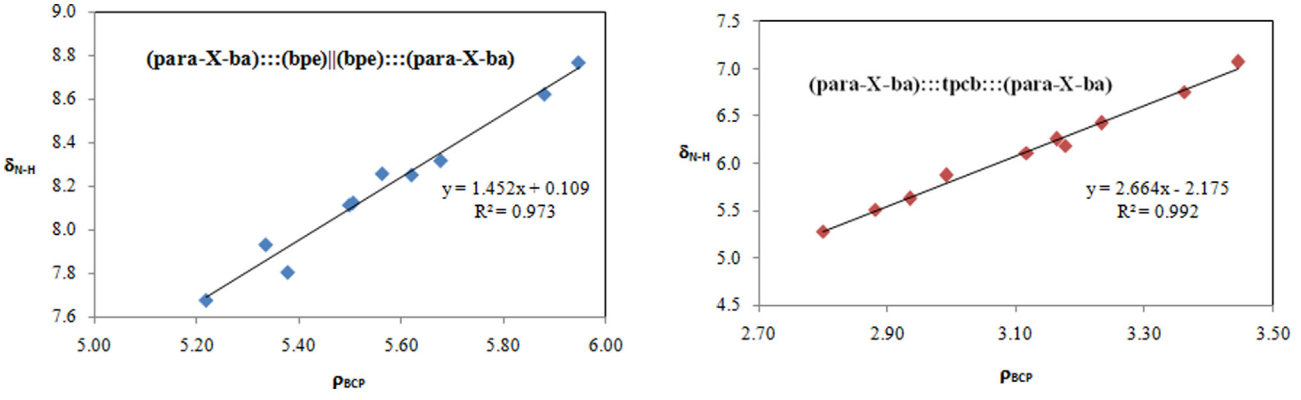

Fig. 4 Correlation between $\delta_{N\text{-}H}$ and ρ_{BCP} for (para-X-ba):::(bpe)||(bpe):::(para-X-ba) (left) and (para-X-ba):::tpcb:::(para-X-ba) (right) complexes.

points (CPs) are evaluated by means of the AIM approach at the M05-2X/6–311 + + G** level for the studied complexes.

Moreover, we have found that the sign of the Laplacian of the electron density at the bond critical point ($\nabla^2\rho$) and that of the energy density (H) could characterize the strength of hydrogen bonding interaction. If the classification of Rozas et al. (Rozas et al., 2000) has been corrected for individual interactions in hydrogen bonding interactions. Thus, weak hydrogen bonding show both $\nabla^2\rho_{BCP}$ and $H_{BCP} > 0$, and medium hydrogen bonding show $\nabla^2\rho_{BCP} > 0$ and $H_{BCP} < 0$, while strong hydrogen bonding show both $\nabla^2\rho_{BCP}$ and $H_{BCP} < 0$. In these interactions, with regard to $\nabla^2\rho_{BCP} > 0$ and $H_{BCP} < 0$ at BCPs in the complexes, they will be classified as medium hydrogen bonding interaction (see Table 3).

7. Conclusion

The computational work that was done in this study complements and extends the general research on the prediction of binding energy (Alvarado et al., 2018); chemical shielding and electron density of (para-X-ba):::(bpe)||(bpe):::(para-X-ba) and (para-X-ba):::tpcb:::(para-X-ba) complexes.

It was found that the hydrogen bonds and π-π stacking in (para-X-ba):::(bpe)||(bpe):::(para-X-ba) and (para-X-ba):::tpcb:::(para-X-ba) complexes with electron-withdrawing substituents were generally observed better activities than the one with electron-donating substituents. Complexes involving electron withdrawing substituents obtained more favorable binding energy values than those involving electron donating substituents. (para-NO_2-ba):::(bpe)||(bpe):::(para-NO_2-ba) Complex involving NO_2 obtained the largest interaction energy value of the study (-38.84 kcal/mol). On the contrary, (para-NH_2-ba):::(bpe)||(bpe):::(para-NH_2-ba) complex involving the NH_2 substituent obtained the lowest interaction energy value of the study (−34.10 kcal/mol).

The hydrogen bond interaction was further proven by ^{1}H NMR. A clear upfield shift (from $\delta_{N\text{-}H}$ = 7.68 to 8.77 ppm in (para-X-ba):::(bpe)||(bpe):::(para-X-ba) complexes) and (from $\delta_{N\text{-}H}$ = 5.29 to 7.07 ppm in (para-X-ba):::tpcb:::(para-X-ba) complexes) of the $\delta_{N\text{-}H}$ proton signal was observed after complextion with electron-withdrawing, indicating these substituents is making the hydrogen bond stronger. The system bearing the electron withdrawing substituents yields an increase of the corresponding $\delta_{N\text{-}H}$. It was demonstrated that for these complexes with electron donating, the calculated shielding of the proton engaged in the hydrogen bonding $\delta_{N\text{-}H}$ was reduced. The ρ_{BCP} increases in the complexes having electron-donating or withdrawing substituents and the calculated ρ_{BCP} values suggest that –NO_2 substituent has the maximum ρ_{BCP} for both (para-X-ba):::(bpe)||(bpe):::(para-X-ba) and (para-X-ba):::tpcb:::(para-X-ba) complexes, it is clear that this substituent is making the hydrogen bond stronger. The maximum value of H shielding is accompanied by the highest ρ_{BCP} hydrogen bond lengths (see Fig. 4).

References

Alvarado, G.C., Brannan, A.D., Swenson, D.C., MacGillivray, L.R., 2018. Org. Lett. 20, 5490–5492.

Biegler Konig, F.W., Schonbohm, J., Bayles, D., AIM2000, 2001. J. Comput. Chem. 22, 545–559.

Boys, S.B., Bernardi, F., 1970. Mol. Phys. 19, 553–566.

Burley, S.K., Petsko, G.A., 1985. Science 229, 23.

Campos-Gaxiola, J.J., Vega-Paz, A., Román-Bravo, P., Höpfl, H., Sánchez-Vázquez, M., 2010. Cryst. Growth Des. 10, 3182–3190.

Chen, S., Ai, L., Zhang, T., Liu, P., Liu, W., Pan, Y., Liu, D., 2020. Arabian J. Chem. 13, 2982–2994.

Chen, Z., Wannere, C.S., Corminboeuf, C., Puchta, R., Schleyer, P.V. R., Chem. Rev.

Corbett, P.T., Leclaire, J., Vial, L., West, K.R., Wietor, J.L., Sanders, J.K.M., Otto, S., 2006. Chem. Rev. 106, 3652–3711.

Cuenca, A.B., Zigon, N., Duplan, V., Hoshino, M., Fujita, M., E. Fernańdez, 2016. Chem.- Eur. J. 22, 4723–4726.

Cyrański, M.K., Jezierska, A., Klimentowska, P., Panek, J.J., Sporzyński, A., 2008. J. Phys. Org. Chem. 21, 472.

Das, A., Watanabe, K., Morimoto, H., Ohshima, T., 2017. Org. Lett. 19, 5794–5797.

Diemoz, K.M., Franz, A.K., 2019. J. Org. Chem. 84, 1126–1138.

Ebrahimi, A., Habibi, M., Neyband, R.S., Gholipour, A.R., 2009. Phys. Chem. Chem. Phys. 11, 11424–11431.

Ebrahimi, A., Habibi, M., Gholipour, A.R., Masoodi, H., 2009. Theor. Chem. Acc. 124, 115–122.

Fujita, N., Shinkai, S., James, T.D., 2008. Chem. Asian J. 3, 1076–1091.

Ghafari, S., Gholipour, A., 2015. J. Mol. Model. 21, 253–259.

Ghafari, S., Gholipour, A., 2019. Chem. Phys. Lett. 721, 91–98.

Hall, D.G., 2006. Boronic Acids: Preparation, Applications in Organic Synthesis and Medicine. John Wiley & Sons.

Hall, D.G., 2005. In Boronic Acids-Preparation and Applications in Organic Synthesis and Medicine. Hall, D.G., (Ed.), Wiley-VCH: Weinheim, pp. 1–26.

Hammett, L.P., 1935. Chem. Rev. 17, 125–136.

Hughes, R.M., Waters, M.L., 2006. Curr. Opin. Struct. Biol. 16, 514.

Iribarren, I., Montero-Campillo, M.M., Alkorta, I., Elguero, J., Quinonero, D., 2019. Phys. Chem. Chem. Phys. 21, 5796–5802.

James, T.D., 2016. Beilstein J. Org. Chem. 12, 391–405.

Kubo, Y., Nishiyabu, R., James, T.D., 2015. Chem. Commun. 51, 2005–2020.

Li, C., Wang, J., Barton, L.M., Yu, S., Tian, M., Peters, D.S., Kumar, M., Yu, A.W., Johnson, K.A., Chatterjee, A.K., Yan, M., Baran, P.S., 2017. Science 356, 7355–7362.

Meyer, E.A., Castellano, R.K., Diederich, F., 2003. Angew. Chem. Int. Ed. 42, 1210.

Nishiyabu, R., Kubo, Y., James, T.D., Fossey, J.S., 2011. Chem. Commun. 47, 1124–1150.

Pecsi, I., Leveles, I., Harmat, V., Vertessy, B.G., Toth, J., 2010. Nucleic Acids Res. 38, 7179.

Quinonero, D., Frontera, A., Deya, P., Alkorta, I., 2008. J. Elguero Chem. Phys. Lett. 460, 406–410.

Rettig, S.J., Trotter, J., 1977. Can. J. Chem. 55, 3071.

Rozas, I., Alkorta, I., Elguero, J., 2000. J. Am. Chem. Soc. 122, 11154–11161.

Saleem, M., Wang, L., Yu, H., Abdin, Z., 2019. Arab. J. Chem. 12, 800–815.

Schleyer, P.V.R., Jiao, H., 1996. Pure Appl. Chem. 68, 209–218.

Schleyer, P.V.R., Maerker, C., Dransfeld, A., Jiao, H., Van Eikema Hommes, N.J.R., 1996. J. Am. Chem. Soc. 118, 6317–6318.

Schmidt, M.W., Baldridge, K.K., Boat, J.A., Elbert, S.T., Gordon, M. S., Jensen, J.H., Koseki, S., Matsunaga, N., Nguyen, K.A., Su, S.J., Windus, T.L., Dupuis, M., Montgo Mery, J.A., 1993. J. Comput. Chem. 14, 1347–1363.

Shang, J., Wang, Y., Chen, M., Dai, J., Zhou, X., Kuttner, J., Hilt, G., Shao, X., Gottfried, J.M., Wu, K., 2015. Nat Chem. 7, 389–393.

Zhao, H., Song, X., Aslan, H., Liu, B., Wang, J., Wang, L., Besenbacher, F., Dong, M., 2016. Phys. Chem. Chem. Phys. 18, 14168–14171.

Zhao, Y., Truhlar, D.G., 2008. Theor Chem Account 120, 215–241.

Zheng, H., McDonald, R., Hall, D.G., Chem. Eur. J. 16 (2010) 5454−5460.

Zheng, H., Ghanbari, S., Nakamura, S., Hall, D.G., 2012. Angew. Chem. Int. Ed. 51, 6187–6190.

Zhikol, O., Shishkin, O., Lyssenko, K., Leszczynski, J., 2005. J. Chem. Phys. 122. 144104-1–144104-144111.

Zhu, W., Tan, X., Shen, J., Luo, X., Cheng, F., Mok, P.C., Ji, R., Chen, K., Jiang, H., 2003. J. Phys. Chem. A 107, 2296–2303.